Optimal Time-Entropy Bounds and Speed Limits for Brownian Thermal Shortcuts

Luís Barbosa Pires,[1] Rémi Goerlich,[2,1] Arthur Luna da Fonseca,[3,1] Maxime Debiossac,[4] Paul-Antoine Hervieux,[2] Giovanni Manfredi,[2,*] and Cyriaque Genet[1,†]

[1]*University of Strasbourg and CNRS, CESQ and ISIS, UMR 7006, F-67000 Strasbourg, France*
[2]*University of Strasbourg and CNRS, Institut de Physique et Chimie des Matériaux de Strasbourg, UMR 7504, F-67000 Strasbourg, France*
[3]*Instituto de Fisica, Universidade Federal do Rio de Janeiro, Caixa Postal 68528, Rio de Janeiro, Rio de Janeiro, 21941-972, Brazil*
[4]*Vienna Center for Quantum Science and Technology, Faculty of Physics, University of Vienna, A-1090 Vienna, Austria*

(Received 22 February 2023; accepted 20 July 2023; published 1 September 2023)

By controlling the variance of the radiation pressure exerted on an optically trapped microsphere in real time, we engineer temperature protocols that shortcut thermal relaxation when transferring the microsphere from one thermal equilibrium state to another. We identify the entropic footprint of such accelerated transfers and derive optimal temperature protocols that either minimize the production of entropy for a given transfer duration or accelerate the transfer for a given entropic cost as much as possible. Optimizing the trade-off yields time-entropy bounds that put speed limits on thermalization schemes. We further show how optimization expands the possibilities for accelerating Brownian thermalization down to its fundamental limits. Our approach paves the way for the design of optimized, finite-time thermodynamics for Brownian engines. It also offers a platform for investigating fundamental connections between information geometry and finite-time processes.

DOI: 10.1103/PhysRevLett.131.097101

The time needed for a body to thermalize with its environment is a natural constraint for operating many physical systems and devices. Controlling thermalization has emerged as one salient challenge in the mesoscale and nanoscale regimes [1–5]. At such scales, the methods of stochastic thermodynamics have proven their efficiency, capable of extending the concepts of work, heat, and entropy to single, fluctuating systems [6,7]. Experimentally, new strategies have recently been implemented on optically trapped Brownian particles to emulate effective and, thereby, controllable thermal baths [8–12]. The fine control of the time dependence of effective temperatures has led to the definition of thermal protocols and optimized cycles [13–15]. Exploiting finite-time thermodynamics, these strategies have also provided the means to circumvent natural thermalization by proposing accelerated paths that a Brownian system can be forced to follow [10,16–21]. Such means form a major topic of current research in the realm of shortcuts to adiabaticity [22,23].

Obviously, speeding-up transitions from one equilibrium state to another demands following nonequilibrium paths that have a thermodynamic cost. Once such cost is evaluated, the design of protocols that optimize the mutually exclusive relation between the rate of acceleration and the energetic expense should be possible. There is a variety of approaches proposed for evaluating that energetic expense [24–30], but the challenge remains to identify the proper one which makes it possible to treat duration and cost on an equal footing, the prerequisite for this optimization [31–33].

In this Letter, we set up a bath engineering strategy involving radiation pressure to directly control the kinetic temperature of an optically trapped, overdamped, Brownian microsphere [34]. This control allows us to impose abrupt transfers from one to another equilibrium state, either increasing or decreasing the temperature down to a minimum set by room temperature T_R. Such steplike transfers are followed by thermal relaxations measured precisely through the diffusive dynamics of the microsphere inside the harmonic optical trap. Our strategy gives the possibility of accelerating such thermal relaxation processes by imposing an overshoot in temperature during the transfer. This leads us to extend to isochoric transitions the engineered swift equilibration (ESE) processes developed so far for isothermal transitions [35]. We show how thermal ESE protocols—hereafter named ThESE protocols—do accelerate thermalization, and experimentally demonstrate the shortening of the duration of initial-to-final thermal equilibrium transfers. We further quantify the thermodynamic cost of this acceleration in terms of entropy production.

The identification of the entropic cost of a thermal shortcut brings us, in the context of harmonic trapping, to a class of optimal thermal protocols, defined as those

protocols that speedup thermalization while minimizing the associated production of entropy. Such isochoric protocols are of a different nature, compared to the isothermal optimal processes we recently derived [33]. In contrast to isothermal processes, whose energetics description only relies on the first law of thermodynamics, the trade-off involved in thermal optimization procedures results in time-entropy bounds that limit the speed of physically realizable thermal protocols. Such limits display a remarkable asymmetry between heating and cooling protocols. Then, we demonstrate that optimal cooling gives access to higher acceleration rates that are unreachable using standard overshooting, ThESE-like protocols. Next, these results are discussed from an energetic viewpoint for the three families (steplike, ThESE, and optimized) of state-to-state transitions, which clarifies the different contributions to the global intake of heat by the trapped microsphere under the action of the fluctuating radiation pressure. Finally, we stress that our optimization-under-cost constraint leads to results that are different from the thermal brachistochrones recently proposed in [21].

Our experiment consists of a single microsphere trapped in an optical tweezer and evolving in a harmonic potential [36,37]. The microsphere diffuses in water with a Stokes drag $\gamma = 2.695 \times 10^{-8}$ kg/s at room temperature $T_R = 293$ K. The trap is characterized by a stiffness $\kappa = 13.1 \pm 0.2$ fN/nm and the overdamped diffusion dynamics by a relaxation time $\tau = \gamma/\kappa = 2.06 \pm 0.04$ ms. As described in detail in the Supplemental Material (Secs. A and B, [38]), an additional radiation pressure is exerted on the sphere by a pushing laser whose intensity $I(t) = I_0 + \delta I(t)$ is digitally controlled over time by an acousto-optic modulator [34]. When $\delta I(t)$ is random (white noise spectrum), this radiation pressure increases the motional variance of the center-of-mass motion of the sphere along the optical axis of the trap. By building a statistical ensemble $\{j\}$ of 1.7×10^4 diffusing trajectories $x_j(t)$, we extract an ensemble average variance $s(t) = \langle x_j^2(t) \rangle$ in direct relation with the pushing laser intensity variance $\langle \delta I^2(t) \rangle$. This random forcing of the microsphere can be interpreted as emulating an effective thermal bath whose temperature $T(t)$ can be set instantaneously in strict relation with the intensity variance with $T(t) \propto \langle \delta I^2(t) \rangle$. The mechanical response of the microsphere is measured through the time evolution of $s(t)$ according to (see Supplemental Material, Sec. C, [38])

$$\frac{ds(t)}{dt} = \frac{2}{\tau}\left(\frac{k_B T(t)}{\kappa} - s(t)\right). \tag{1}$$

The effective nature of $T(t)$ implies that thermal changes impact the diffusion coefficient simply as $D(t) = k_B T(t)/\gamma$ and the system relaxation time τ remains constant. Thus, by transforming temperature into an external control parameter $T(t)$, the crucial asset of our bath engineering strategy

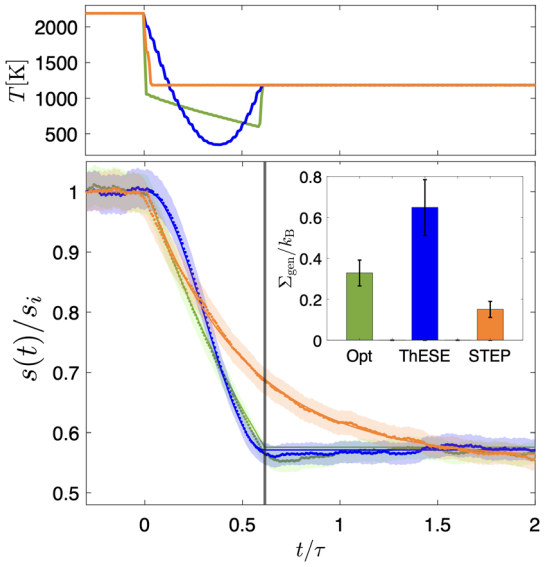

FIG. 1. Upper panel: Time evolution $T(t)$ plotted for three cooling protocols connecting two thermal equilibrium states, one initial at $T_R + T_i$ and one final at $T_R + T_f$ where $T_R = 293$ K corresponds to room temperature and $T_R + T_i = 2200$ K, $T_R + T_f = 1200$ K to the target temperatures fixed by the laser fluctuation spectrum. The orange curve corresponds to a steplike protocol (STEP) with a simple temperature discontinuous quench, the blue curve to the ThESE protocol through which T_i and T_f are connected by a third degree polynomial, the green curve to the optimal protocol (Opt) with its two discontinuities ensuring the connection between the initially hot (at $t = 0^-$) and finally cold (at $t = \Delta t^+$) equilibrium states. Lower panel: Measured time evolutions (data points with same color coding as in the upper panel) of the motional variances $s(t)$ induced by the different thermal protocols starting at $t = 0^+$. The variances for the ThESE and Opt shortcuts reach equilibrium at a rate $\Delta t/\tau = 0.6$, as indicated by the vertical line. The shaded areas give the experimental errors at a 95% confidence interval for $s(t)$. The analytical solutions for $s(t)$ for the three protocols, calculated in the Supplemental Material (Sec. E, [38]) from Eq. (1), correspond to the continuous lines drawn on the experimental data points. Inset: Levels of produced entropy Σ_{gen} associated to each of the three protocols and evaluated using Eq. (2). Error bars for Σ_{gen} correspond to the combination of the uncertainties in $s(t)$, stiffness and temperature (see more details in the Supplemental Material, Sec. H, [38]).

is the possibility of performing specific temperature *protocols* that can be arbitrarily fast from one initial $T_R + T_i$ to another final target temperature $T_R + T_f$. As discussed below, this opens rich analogies with recent works that have demonstrated how time-dependent optical trap stiffness protocols $\kappa(t)$ can shortcut, engineer, and even optimize state-to-state isothermal processes [33,35,41].

Let us start by implementing a sudden, steplike change $\Delta T = T_f - T_i$ between an initial $T_R + T_i$ and a final $T_R + T_f$ temperature. This steplike protocol (STEP) is described in the upper panel of Fig. 1. It produces a transient response of the variance $s(t)$ that we measure and

plot in the lower panel of Fig. 1. As observed in excellent agreement with Eq. (1), the variance relaxes toward the new thermal equilibrium state with a relaxation time 2τ. Such a relaxation corresponds to the definition of natural thermalization, in which the system is left free to evolve toward a new equilibrium state. Now, we show that it is possible to impose a temperature protocol that displays a much shorter thermalization time for the same ΔT change. To do so, we extend to temperature the class of ESE isothermal protocols presented in [35] with a polynomial temperature overshoot evaluated in the Supplemental Material (Sec. E.2, [38]), imposing stationary thermal equilibrium $s_i/s_f = (T_R + T_i)/(T_R + T_f)$ and $\dot{s}(t)|_{t=0,\Delta t} = 0$ at the initial $s(t=0) = s_i$ and final $s(t=\Delta t) = s_f$ steps of the process. The corresponding $T(t)$ protocol is plotted in the upper panel of Fig. 1 for a chosen transfer duration $\Delta t = 1.23$ ms imposed to be shorter than 2τ with a ratio $\Delta t/\tau = 0.6$. It is implemented experimentally, and we measure in the lower panel of Fig. 1 the time evolution of the system's variance $s(t)$ in excellent agreement with the theory.

The remaining central question for such accelerated thermalization protocols concerns their possible optimization with respect to a well-identified footprint. In the case of isothermal stiffness protocols $\kappa(t)$, the thermodynamic cost of acceleration was evaluated through the associated work expense and the minimization procedure designed accordingly [31–33]. Temperature protocols, in contrast, are entropic by nature and have been recently characterized using the concept of thermal (entropic) work [5]. This entropic nature clearly appears when interpreting Eq. (1) thermodynamically: whenever the temperature changes faster than τ, the system will evolve along an irreversible, nonequilibrium process in which the instantaneous variance $s(t)$ will be different from the one expected by equipartition. Thus, the difference between $s(t)$ and $k_B T(t)/\kappa$ measures the deviation from a reversible process and, as such, is associated to a given production of entropy that we evaluate now.

For our experiments, we define the system's stochastic entropy $\sigma_{\rm sys}[x_j(t), T(t)] = -k_B \ln p[x_j(t), T(t)]$ [7] from an extension of the Boltzmann probability density $p[x_j(t), T(t)] = \sqrt{\kappa/2\pi k_B T(t)}\, \exp\{-\kappa x_j^2(t)/[2k_B T(t)]\}$ to nonequilibrium processes that connect two equilibrium states. This definition of entropy has appropriate thermodynamic features, as discussed in the Supplemental Material, Sec. D, [38]. Using this definition, the infinitesimal variation of the system's entropy is evaluated as $d\sigma_{\rm sys}[x_j(t), T(t)] = \kappa x_j dx_j/T(t) + [k_B T(t) - \kappa x_j^2] dT/[2T^2(t)]$. The first term involves the quantity of heat $dq = -\kappa x_j dx_j$ associated with the change of internal energy of the system. It corresponds to (the opposite of) the variation of the entropy of the medium $đ\sigma_{\rm med} = dq/T(t)$ where we use the đ notation for nonexact differentials. Thus, the second term, written as $đ\sigma_{\rm gen} = d\sigma_{\rm sys} + đ\sigma_{\rm med}$, gives the infinitesimal amount of total entropy generated along the elementary path dT.

The generated total entropy, once ensemble averaged $\langle đ\sigma_{\rm gen}\rangle = [k_B T(t) - \kappa\langle x_j^2(t)\rangle] dT/[2T^2(t)]$ and cumulated from the initial time $t = 0$ to a given time t of the isochoric transformation becomes

$$\Sigma_{\rm gen}(t) = \frac{1}{2}\int_0^t \frac{\dot{T}(\zeta)}{T^2(\zeta)}[k_B T(\zeta) - \kappa s(\zeta)] d\zeta, \qquad (2)$$

where the nonequilibrium nature of the transformation is imprinted in the difference $k_B T(t) - \kappa s(t)$ between the measured variance and equipartition. Therefore, $\Sigma_{\rm gen}(t)$ corresponds to the cumulated entropy produced along the irreversible transition and constitutes the entropic footprint of a finite-time isochoric process. For the entire STEP and ThESE protocols, in which $t \to \infty$ and $t = \Delta t$, respectively, the total entropy production can be easily calculated using Eq. (2), and the results are plotted in the inset of Fig. 1. When compared, these values reveal, in a striking manner, the entropic cost of thermal acceleration with $\Sigma_{\rm gen}^{\rm ThESE} > \Sigma_{\rm gen}^{\rm STEP}$.

Our analysis now gives the possibility of deriving the actual temporal profile of an optimal protocol that minimizes this entropic cost for a given choice of transfer duration Δt from one equilibrium state at $T_R + T_i$ to another at $T_R + T_f$. Extending to entropic cost the minimization procedure we developed in [33], we build a functional that combines on an equal footing the transfer duration and the corresponding generation of entropy

$$J[T(s)] = \int_{s_i}^{s_f} \left(\frac{\gamma}{k_B T(s) - s\kappa} - \lambda \frac{\kappa}{k_B T(s)}\right) ds, \qquad (3)$$

where the first term on the right-hand side is the transfer duration expressed as a function of the variance according to Eq. (1). The second term is the path dependent part of the generated entropy, evaluated by integrating by parts Eq. (2). The derivations of these expressions for the transfer duration and generated entropy are detailed in the Supplemental Material, Sec. E.3, [38]. We introduce a Lagrange multiplier λ to regulate the trade-off between the two quantities. The optimization procedure consists in searching for the paths in the $[s, T(s)]$ space that minimize $J[T(s)]$ under the constraint that the system is at thermodynamic equilibrium at the initial and final times. As explained in the Supplemental Material, Sec. E, [38], the procedure yields two families of optimized thermal protocols $T_{\rm heat/cool}(s)$ associated, respectively, to heating $T_i < T_f$ and cooling $T_i > T_f$. We emphasize that the $T_{\rm heat/cool}(s)$ protocol does not satisfy thermal equilibrium at both initial and final times and, therefore, must be supplemented by two discontinuous transitions, as in the case of optimal isothermal processes [31,33]. During the interval Δt, those

two solutions correspond to an exponential evolution of the variance with $s_{\rm opt}(t) = s_i[(T_R + T_f)/(T_R + T_i)]^{t/\Delta t}$. It is remarkable that both $T_{\rm heat/cool}(s)$ protocols can be described with a single expression

$$T_{\rm opt}(t) = \frac{\kappa s_{\rm opt}(t)}{k_{\rm B}}\left(1 + \frac{\tau}{k_{\rm B}}\frac{\Delta\Sigma_{\rm sys}}{\Delta t}\right) \tag{4}$$

where $\Delta\Sigma_{\rm sys} = k_{\rm B}\ln[(T_R + T_f)/(T_R + T_i)]/2$ is the protocol-independent total variation in the entropy of the system. This expression is plotted in the upper panel of Fig. 1 for an optimal cooling protocol and with the same shortening rate $\Delta t/\tau = 0.6$ as the ThESE protocol discussed above. As one expected important result of our work, $\Sigma_{\rm gen}^{\rm ThESE} > \Sigma_{\rm gen}^{\rm opt}$.

The optimal protocol given by Eq. (4) together with $s_{\rm opt}(t)$ injected into Eq. (2) leads us to evaluate (see Supplemental Material, Sec. F [38]) the minimal entropy produced through an isochoric transformation of duration Δt as

$$\Sigma_{\rm min} = \frac{\Delta\Sigma_{\rm sys}}{1 + \frac{k_{\rm B}}{\tau}\frac{\Delta t}{\Delta\Sigma_{\rm sys}}}, \tag{5}$$

an expression valid both for cooling and heating protocols but with different consequences, as discussed below.

In Fig. 2, we plot Eq. (5) for cooling (upper panel) and heating (lower panel) optimal protocols (solid black lines). The curves draw exclusion regions for entropy production that correspond to the minimal amount of entropy that can be generated in an isochore for a given Δt: thus, they correspond to optimal time-entropy bounds. Our experimental results obtained for different optimal cooling and heating protocols $T_{\rm opt}(t)$ injected within our optical trap (same set of temperatures but different transfer durations) all precisely fall on the expected bounds.

For a cooling process with $\Delta\Sigma_{\rm sys} < 0$, Eq. (5) also puts an asymptotic limit to the transfer rate with a minimal transfer duration of $\Delta t_{\rm min}/\tau = -\Delta\Sigma_{\rm sys}/k_{\rm B}$. This limit is in agreement with the one-dimensional cooling brachistochrone result given in [21]. Beyond this minimum, our approach yields bounds on the dynamical evolution of our system, extracted from the trade-off involved in the optimization procedure between the transfer duration and the production of entropy. Such bounds must be considered as true speed limits on the state-to-state connection [42]. They are directly associated with a divergence in the entropic cost as clearly seen experimentally in Fig. 2 for the shortest transfer rate that we probed (vertical dashed line). This limit in the cooling acceleration is directly related to the fact that the lowest temperature reached right before the final discontinuity at $t = \Delta t^-$ (see Fig. 1, upper panel) $T_{\rm min} = T_{\rm opt}(\Delta t^-) = T_f[1 + (\tau/k_{\rm B})(\Delta\Sigma_{\rm sys}/\Delta t)]$ which the optimal protocol passes through, cannot be smaller than 0 K, a temperature limit reached when

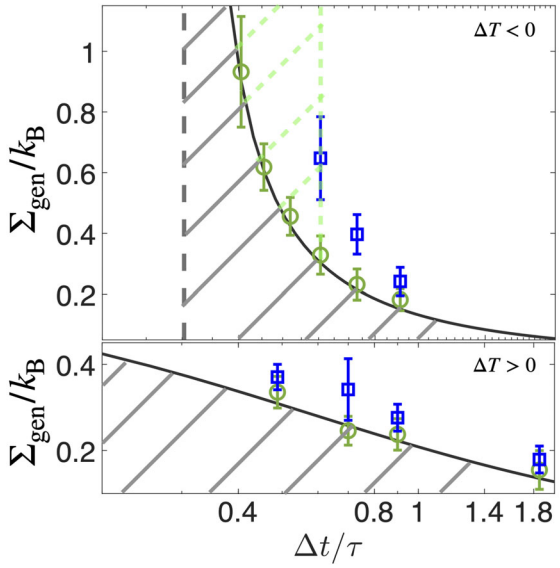

FIG. 2. Minimal time-entropy bound (solid black lines) corresponding to an optimal cooling ($T_R + T_i = 2200$ K, $T_R + T_f = 1200$ K) protocol (upper panel) and an optimal heating protocol performed between $T_R + T_i = 350$ K to $T_R + T_f = 1100$ K (lower panel). The gray hatched region is forbidden to any acceleration method. Experimental measurements for optimal protocols are shown with green open circles and with blue open squares for ThESE protocols. Error bars correspond to experimental errors propagated through Eq. (2) at a 95% confidence level. Because room temperature is a bound for all our experiments, the fundamental limit put on ThESE cooling protocols is set at $\Delta t/\tau = 0.6$ for the chosen experimental parameters. This limit is depicted as a second exclusion region (green hatched region) for such overshooting temperature protocols.

$\Delta t_{\rm min}/\tau = -(\Delta\Sigma_{\rm sys}/k_{\rm B}) = 0.3$ for our (T_i, T_f) choice. However, experimentally, we necessarily have $T_{\rm min} \geq T_R$, and for the case presented in Fig. 2, this implies that the shortest transfer rate reachable is $\Delta t_{\rm min}/\tau = -(\Delta\Sigma_{\rm sys}/k_{\rm B})(1 + T_{\rm R}/T_f)$.

Room temperature obviously bounds from below all overshoot temperatures that can be physically hit. This leads to an interesting consequence when comparing optimal and ThESE cooling protocols for identical shortening rates and target temperatures $T_i > T_f$. Because the overshoot temperature for the ThESE protocol is necessarily lower than $T_{\rm min}$ for the optimal protocol for a given Δt—see Fig. 1 (upper panel)—the room temperature bound is reached by the ThESE protocol before the optimal one. More precisely, the ThESE protocol cannot accelerate cooling beyond $\Delta t/\tau = 0.6$, since this would imply an overshoot temperature below room temperature. This physical limit put on the ThESE protocol corresponds to the sharp exclusion region plotted in Fig. 1 (upper panel). In contrast and remarkably, the optimal protocols can still have access to stronger acceleration rates with ratios between $\Delta t/\tau = 0.6$ and 0.4 that remain available experimentally, as we perfectly measure. This important result

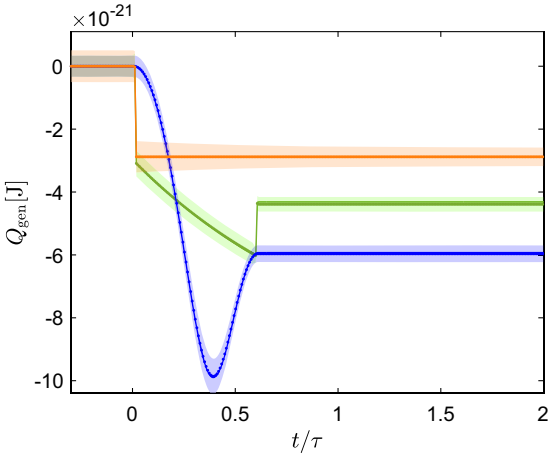

FIG. 3. Ensemble average, time-dependent cumulative generated heats $Q_{\rm gen}$ for a STEP (orange), a ThESE (blue) and an optimal protocol (green), all set for an initial time $t = 0$ ms. Same color coding as in Fig. 1 and same shaded areas associated with experimental errors at a 95% confidence level, including calibration and temperature uncertainties evaluated by the expression of $Q_{\rm gen}(t)$.

reveals another, yet unexpected, thermodynamic advantage of optimization giving access to time-entropy regions that are simply forbidden to nonoptimized protocols.

Contrasting with cooling, optimal heating protocols are not constrained by any fundamental limit (Fig. 2, lower panel). With $\Delta\Sigma_{\rm sys} > 0$ in Eq. (5), the production of entropy does not diverge and the system can be forced to thermalize arbitrarily fast, a feature also found in the brachistochrone case [21]. The optimal time-entropy bound for heating protocols is plotted in Fig. 2 together with the experimental measurements obtained when implementing heating ThESE and optimal protocols.

Finally, we measure the instantaneous, ensemble average, heat generated by the action of the radiation pressure $đQ_{\rm gen} = -T(t)d\Sigma_{\rm gen}$ and transferred to the microsphere while evolving from the initial state $s(t = 0) = s_i$ to one nonequilibrium state $s(t)$ [43]. The time-dependent cumulative intake of heat for isochores can be evaluated directly from Eq. (2) as $Q_{\rm gen}(t) = -\int_0^t d\zeta \dot{T}(\zeta)[k_{\rm B}T(\zeta) - \kappa s(\zeta)]/[2T(\zeta)]$. This quantity of heat is plotted in Fig. 3 for the three families of protocols studied here—STEP, ThESE, and optimal—fixing a shortening ratio of 0.6 for the ThESE and the optimal protocols. The time evolution and the final amount of $Q_{\rm gen}(t)$ strongly depend on the type of protocol. The energetic cost of the STEP protocol is relatively low, but it requires a long thermalization time. When comparing the other two protocols that have the same Δt, it is clear that the optimal solution mitigates the energetic cost of the transfer when compared to the ThESE protocol.

In conclusion, we have used a fluctuating, white-noise, radiation pressure to emulate temperature protocols applied to an optically trapped microsphere and to extend the concept of engineered swift equilibration to thermal protocols. A central result was to identify the entropic cost of these nonequilibrium protocols. As such, these results are not a mere extension of our previous ones on optimal isothermal processes [33]. There, the energetics of an isothermal transformation was straightforward to quantify—and thereby, to optimize—since it only involved the first law of thermodynamics. For thermal protocols, the trade-off between the state-to-state transfer duration and the entropic cost led us to the design of optimal cooling and heating protocols. We identified minimal time-entropy bounds for all possible shortcut strategies in harmonic potentials and derived speed limits on the transfer rates. In addition, an energetic analysis showed how optimization yields the best thermodynamic compromise between acceleration and cost. This optimization is important in the context of thermodynamic cycles and Brownian heat engines, and bears a fundamental appeal considering that the entropic cost can be described as a thermodynamic length [42]. From this perspective, our optimal cooling and heating shortcuts $T_{\rm opt}(t)$ correspond to geodesics within an information geometry viewpoint that draws fascinating connections yet to be further explored [44,45].

This work is part of the Interdisciplinary Thematic Institute QMat of the University of Strasbourg, CNRS, and Inserm. It was supported by the following programs: IdEx Unistra (Grant No. ANR-10-IDEX-0002), SFRI STRATUS Project (Project No. ANR-20-SFRI-0012), and USIAS (Grant No. ANR-10-IDEX- 0002-02), under the framework of the French Investments for the Future Program.

*giovanni.manfredi@ipcms.unistra.fr
†genet@unistra.fr

[1] D. E. Chang, C. A. Regal, S. B. Papp, D. J. Wilson, J. Ye, O. Painter, H. J. Kimble, and P. Zoller, Cavity opto-mechanics using an optically levitated nanosphere, Proc. Natl. Acad. Sci. U.S.A. **107**, 1005 (2010).
[2] I. A. Martínez, É. Roldán, L. Dinis, and R. A. Rica, Colloidal heat engines: A review, Soft Matter **13**, 22 (2017).
[3] J. A. Albay, Z.-Y. Zhou, C.-H. Chang, and Y. Jun, Shift a laser beam back and forth to exchange heat and work in thermodynamics, Sci. Rep. **11**, 4394 (2021).
[4] C. Gonzalez-Ballestero, M. Aspelmeyer, L. Novotny, R. Quidant, and O. Romero-Isart, Levitodynamics: Levitation and control of microscopic objects in vacuum, Science **374**, eabg3027 (2021).
[5] M. Rademacher, M. Konopik, M. Debiossac, D. Grass, E. Lutz, and N. Kiesel, Nonequilibrium Control of Thermal and Mechanical Changes in a Levitated System, Phys. Rev. Lett. **128**, 070601 (2022).
[6] K. Sekimoto, *Stochastic Energetics* (Springer, New York, 2010), Vol. 799.

[7] U. Seifert, Stochastic thermodynamics, fluctuation theorems and molecular machines, Rep. Prog. Phys. **75**, 126001 (2012).

[8] M. G. Raizen, S. Kheifets, and T. Li, Optical trapping and cooling of glass microspheres, in *Optical Trapping and Optical Micromanipulation IX* (SPIE, San Diego, 2012), Vol. 8458, pp. 66–72.

[9] I. A. Martinez, E. Roldán, J. M. R. Parrondo, and D. Petrov, Effective heating to several thousand kelvins of an optically trapped sphere in a liquid, Phys. Rev. E **87**, 032159 (2013).

[10] M. Chupeau, B. Besga, D. Guéry-Odelin, E. Trizac, A. Petrosyan, and S. Ciliberto, Thermal bath engineering for swift equilibration, Phys. Rev. E **98**, 010104(R) (2018).

[11] U. Delić, M. Reisenbauer, K. Dare, D. Grass, V. Vuletić, N. Kiesel, and M. Aspelmeyer, Cooling of a levitated nanoparticle to the motional quantum ground state, Science **367**, 892 (2020).

[12] F. van der Laan, F. Tebbenjohanns, R. Reimann, J. Vijayan, L. Novotny, and M. Frimmer, Sub-Kelvin Feedback Cooling and Heating Dynamics of an Optically Levitated Librator, Phys. Rev. Lett. **127**, 123605 (2021).

[13] I. A. Martínez, É. Roldán, L. Dinis, D. Petrov, J. M. Parrondo, and R. A. Rica, Brownian Carnot engine, Nat. Phys. **12**, 67 (2016).

[14] C. A. Plata, D. Guéry-Odelin, E. Trizac, and A. Prados, Building an irreversible Carnot-like heat engine with an overdamped harmonic oscillator, J. Stat. Mech. (2020) 093207.

[15] G. Watanabe and Y. Minami, Finite-time thermodynamics of fluctuations in microscopic heat engines, Phys. Rev. Res. **4**, L012008 (2022).

[16] A. Kumar and J. Bechhoefer, Exponentially faster cooling in a colloidal system, Nature (London) **584**, 64 (2020).

[17] C. A. Plata, D. Guéry-Odelin, E. Trizac, and A. Prados, Finite-time adiabatic processes: Derivation and speed limit, Phys. Rev. E **101**, 032129 (2020).

[18] K. Nakamura, J. Matrasulov, and Y. Izumida, Fast-forward approach to stochastic heat engine, Phys. Rev. E **102**, 012129 (2020).

[19] Y. Jun and P.-Y. Lai, Instantaneous equilibrium transition for Brownian systems under time-dependent temperature and potential variations: Reversibility, heat and work relations, and fast isentropic process, Phys. Rev. Res. **3**, 033130 (2021).

[20] J.-F. Chen, Optimizing Brownian heat engine with shortcut strategy, Phys. Rev. E **106**, 054108 (2022).

[21] A. Patrón, A. Prados, and C. A. Plata, Thermal brachistochrone for harmonically confined Brownian particles, Eur. Phys. J. Plus **137**, 1 (2022).

[22] D. Guéry-Odelin, A. Ruschhaupt, A. Kiely, E. Torrontegui, S. Martínez-Garaot, and J. G. Muga, Shortcuts to adiabaticity: Concepts, methods, and applications, Rev. Mod. Phys. **91**, 045001 (2019).

[23] D. Guéry-Odelin, C. Jarzynski, C. A. Plata, A. Prados, and E. Trizac, Driving rapidly while remaining in control: Classical shortcuts from Hamiltonian to stochastic dynamics, Rep. Prog. Phys. **86**, 035902 (2023).

[24] J. A. C. Albay, S. R. Wulaningrum, C. Kwon, P.-Y. Lai, and Y. Jun, Thermodynamic cost of a shortcuts-to-isothermal transport of a Brownian particle, Phys. Rev. Res. **1**, 033122 (2019).

[25] M. Debiossac, D. Grass, J. J. Alonso, E. Lutz, and N. Kiesel, Thermodynamics of continuous non-Markovian feedback control, Nat. Commun. **11**, 1360 (2020).

[26] A. Prados, Optimizing the relaxation route with optimal control, Phys. Rev. Res. **3**, 023128 (2021).

[27] A. G. Frim and M. R. DeWeese, Optimal finite-time Brownian Carnot engine, Phys. Rev. E **105**, L052103 (2022).

[28] Z. Ye, F. Cerisola, P. Abiuso, J. Anders, M. Perarnau-Llobet, and V. Holubec, Optimal finite-time heat engines under constrained control, Phys. Rev. Res. **4**, 043130 (2022).

[29] Y. Jun and P.-Y. Lai, Minimal dissipation protocols of an instantaneous equilibrium Brownian particle under time-dependent temperature and potential variations, Phys. Rev. Res. **4**, 023157 (2022).

[30] P. V. Paraguassú, R. Aquino, L. Defaveri, and W. A. M. Morgado, Effects of the kinetic energy in heat for overdamped systems, Phys. Rev. E **106**, 044106 (2022).

[31] T. Schmiedl and U. Seifert, Optimal Finite-Time Processes in Stochastic Thermodynamics, Phys. Rev. Lett. **98**, 108301 (2007).

[32] M. V. S. Bonança and S. Deffner, Minimal dissipation in processes far from equilibrium, Phys. Rev. E **98**, 042103 (2018).

[33] Y. Rosales-Cabara, G. Manfredi, G. Schnoering, P.-A. Hervieux, L. Mertz, and C. Genet, Optimal protocols and universal time-energy bound in Brownian thermodynamics, Phys. Rev. Res. **2**, 012012(R) (2020).

[34] R. Goerlich, L. B. Pires, G. Manfredi, P.-A. Hervieux, and C. Genet, Harvesting information to control nonequilibrium states of active matter, Phys. Rev. E **106**, 054617 (2022).

[35] I. A. Martínez, A. Petrosyan, D. Guéry-Odelin, E. Trizac, and S. Ciliberto, Engineered swift equilibration of a Brownian particle, Nat. Phys. **12**, 843 (2016).

[36] M. J. Padgett, J. Molloy, and D. McGloin, *Optical Tweezers: Methods and Applications* (CRC Press, New York, 2010).

[37] A. Gennerich, *Optical Tweezers* (Springer, New York, 2017).

[38] See Supplemental Material at http://link.aps.org/supplemental/10.1103/PhysRevLett.131.097101 for a schematic presentation of the experimental setup, a presentation of the temperature calibration method, the variance equation of motion, the evaluation of the generated entropy, a detailed description of the different STEP, ThESE, and optimal protocols, the derivation of the optimal production of entropy, the associated energetics, the data analysis, and evaluation of errors, which includes Refs. [33–35,39,40].

[39] K. Berg-Sørensen and H. Flyvbjerg, Power spectrum analysis for optical tweezers, Rev. Sci. Instrum. **75**, 594 (2004).

[40] K. Sekimoto, Langevin equation and thermodynamics, Prog. Theor. Phys. Suppl. **130**, 17 (1998).

[41] A. Le Cunuder, I. A. Martínez, A. Petrosyan, D. Guéry-Odelin, E. Trizac, and S. Ciliberto, Fast equilibrium switch of a micro mechanical oscillator, Appl. Phys. Lett. **109**, 113502 (2016).

[42] N. Shiraishi, K. Funo, and K. Saito, Speed Limit for Classical Stochastic Processes, Phys. Rev. Lett. **121**, 070601 (2018).

[43] The minus sign in this convention means that, for a generation of entropy $d\Sigma_{\mathrm{gen}} > 0$, the energy flows from medium to the system and $đQ_{\mathrm{gen}} < 0$, consistent with the standard convention of stochastic thermodynamics [40].

[44] S. Ito, Stochastic Thermodynamic Interpretation of Information Geometry, Phys. Rev. Lett. **121**, 030605 (2018).

[45] S. Ito, Geometric thermodynamics for the Fokker-Planck equation: Stochastic thermodynamic links between information geometry and optimal transport, Inf. Geom. (2023).